Research Article

Onpreeya Veang-in, Yottha Srithep*, John Morris, Darunee Aussawasathien, and Patnarin Worajittiphon

Stereocomplex PLLA–PBAT copolymer and its composites with multi-walled carbon nanotubes for electrostatic dissipative application

https://doi.org/10.1515/epoly-2023-0089
received June 30, 2023; accepted August 19, 2023

Abstract: Because of its low thermal stability and brittleness, both the drawbacks of poly(L-lactide) (PLLA) were solved by forming stereocomplex (ST) and its copolymer with poly(butylene adipate-*co*-terephthalate) (PLLA–PBAT). In this study, we synthesized PLLA and PLLA–PBAT copolymer by ring-opening polymerization. Both polymers were blended with poly(D-lactide) to form ST crystals. Multi-walled carbon nanotubes (MWCNTs) were added into the polymer matrix at 5 phr by the solvent casting method. The surface resistance of the composite was ≅10^6 Ω, which is appropriate for electrostatic dissipative purposes. The copolymer and its ST crystallites were confirmed by the peaks in infrared spectra at 922 and 908 cm^{-1}, respectively. The PLLA–PBAT copolymer had 60% lower tensile strength than PLLA and its stereocomplex, but 10% higher elongation at break. The elongation at break of the PLLA–PBAT copolymer/MWCNT composite decreased by 17% while its thermal stability slightly increased when compared to the unfilled copolymer. The melting temperature for both ST PLLA–PBAT copolymers, with and without MWCNTs, was around 225°C, which is 50°C higher than that of the homocrystals. Moreover, the glass transition temperature and crystallinity of the ST PLLA–PBAT copolymer also increased by adding MWCNTs.

Keywords: stereo-complex poly(L-lactide) copolymer, poly(D-lactide), poly(butylene adipate-*co*-terephthalate), ring-opening polymerization, multi-walled carbon nanotubes

1 Introduction

Poly(L-lactide) (PLLA) is a biodegradable polymer that can be processed easily and is already marketed. It is formed entirely from renewable resources by bio-conversion or polymerization (1). However, PLLA has structural and physical limitations, which limit its processing, formability, and foaming. It has low heat resistance, low toughness (high brittleness), low melt strength, and a slow crystallization rate (2). Blending PLLA with other polymers can avoid these constraints. Many researchers have used copolymerizing lactides with other monomers and macromolecules or blending PLLA with flexible plasticizers to toughen the polymer (3). Biodegradable aliphatic polyesters used to toughen PLLA were polypropylene carbonate (4,5), poly(butylene adipate-*co*-terephthalate) (PBAT) (6,7), poly(ε-caprolactone) (8), and poly(butylenes succinate) (9). PBAT is viable for strengthening PLLA because of its high toughness and biodegradability (10). The copolymerization reaction of PLLA and PBAT can improve their compatibility. Na et al. showed that bi-, tri-, and multi-block copolymers improved the compatibility of many miscible and partially miscible blending systems (11).

There are two enantiomers of polylactide, PLLA and poly(D-lactide) (PDLA). Stereocomplex (ST) crystals were formed when PLLA and PDLA were blended, which have a melting point of about 225°C or 50°C higher than that of homocrystallized PLLA or PDLA (12). As a result, the

* **Corresponding author: Yottha Srithep,** Manufacturing and Materials Research Unit, Department of Manufacturing Engineering, Faculty of Engineering, Mahasarakham University, Mahasarakham, 44150, Thailand, e-mail: yottha.s@msu.ac.th
Onpreeya Veang-in: Manufacturing and Materials Research Unit, Department of Manufacturing Engineering, Faculty of Engineering, Mahasarakham University, Mahasarakham, 44150, Thailand
John Morris: School of Industrial Education and Technology, King Mongkut's Institute of Technology Ladkrabang, Bangkok, 10520, Thailand
Darunee Aussawasathien: Plastics Technology Lab, Polymer Research Unit, National Metal and Materials Technology Center, Pathumthani, 12120, Thailand
Patnarin Worajittiphon: Department of Chemistry, Faculty of Science, Chiang Mai University, Chiang Mai, 50200, Thailand; Center of Excellence in Materials Science and Technology, Chiang Mai University, Chiang Mai, 50200, Thailand

mechanical, thermal, and biological degradability properties of the ST materials were all improved. According to Jiang et al. (13), the formation of an ST structure considerably raised the melting point, crystallization temperature, and overall degree of crystallization significantly. Srisuwan and Baimark (14) presented that the stereocomplexation, heat resistance, and mechanical properties of PLLA/PDLA-blended films may be controlled by the molecular weight of PDLA. The low molecular weight PDLA made complete ST, fast crystallization, and had good heat resistance, but high brittleness. Meanwhile, high molecular weight PDLA simultaneously improved the mechanical characteristics of the ST while suppressing stereocomplexation, crystallization, and heat resistance. Chen et al. (15) devised a workable and reliable method for creating a stable continuous PLLA/PBAT (70/30) mixture at the nanoscale. Because of grafting reactions and H-bonding contacts between PDLA grafts and PLLA chains during reactive blending, ST crystals were generated *in situ*. Furthermore, they demonstrated that the *in situ* generated nucleation agent (i.e., the ST) was responsible for a large increase in the crystallization rate of the PLLA matrix. Thus, the ST served as a rigid supporting layer between phases even above 200°C, leading to noticeably improved stability in the melt.

Because of their high electrical and thermal conductivity, carbon nanotubes (CNTs) have been proposed as nanofillers in polymer composites. There are three types of CNTs, single-walled carbon nanotubes (SWCNTs), double-walled carbon nanotubes (DWCNTs), and multi-walled carbon nanotubes (MWCNTs) (16). MWCNTs are recognized for their strengths which range between 2.5 and 3.5 GPa and they are typically used to enhance the mechanical properties of polymer composites (17). Unlike SWCNTs and DWCNTs, MWCNTs with different structures are readily available commercially. MWCNTs have been widely used as conductive nanofillers due to their low cost, wide variety, greater availability, and ease of dispersion (18). Therefore, developing thin conductive polymer films requires understanding the effects of the structure and composition of conductive fillers on the electrical and mechanical properties of the final composite films. MWCNTs have a high aspect ratio, surface area, Young's modulus, and excellent electrical and thermal properties which make them ideal for producing ultra-lightweight and extremely strong composites (19,20).

Research on PLLA/CNT composites has mainly been directed at enhancing mechanical properties, crystallization, and electrical conductivity. However, the composites do not possess flexibility and heat resistance (21). In this work, we report the ST PLLA–PBAT copolymer/MWCNT nanocomposites, prepared from the PLLA–PBA copolymer, PDLA, and MWCNT blends. We examined how the ST formation and MWCNT addition affected the chemical structure, electrical resistivity, and thermal and mechanical properties of polymer nanocomposites. First, we enhanced the flexibility of the PLLA matrix by synthesizing PLLA–PBAT copolymer (22). After that, the PLLA–PBAT copolymer was blended with PDLA in a 1:1 weight ratio to increase its thermal properties. Similar to our previous work, the blending of PLLA with PDLA led to the formation of an ST, which had a melting temperature of around 225°C, 50°C higher than that of homocrystallized PLLA or PDLA (12). The ST copolymer was blended with MWCNTs to create an electrostatic dissipative (ESD)-suitable conductive composite film. To the best of our knowledge, there are no literature reports on the ST of the PLLA–PBAT copolymer/MWCNT nanocomposite so far.

2 Materials and methods

2.1 Materials

L-Lactide (98% L-lactide) and PDLA (Luminy® D120) were received from Total Corbion Thailand Ltd. 1-Dodecanol (98%) was purchased from Across Co. Ltd. PBAT (ecoflex® F blend C1200) was sourced from BASF SE, Deutschland. MWCNTs (HDPlas® MWCNT-O_2) were purchased from Haydale Technologies (Thailand) Co., Ltd. Stannous octanoate ($Sn(Oct)_2$) was provided by Sigma-Aldrich. Chloroform (CH_3Cl, AR grade) was obtained from RCI Labscan, Thailand.

2.2 Synthesis of PLLA and PLLA–PBAT copolymer

We prepared PLLA and PLLA–PBAT from L-lactide monomers. L-Lactide was dried in a vacuum oven at 50°C, 12 h before use. PLLA was synthesized using 0.1 mol% 1-dodecanol as an initiator, while the synthesis of the copolymer PLLA–PBAT required using 0.01 mol% PBAT as an initiator (lactide 40 g, PBAT 13.7828 g). For the preparation of both samples, 0.05 mol% $Sn(Oct)_2$ was used as a catalyst. PLLA and PLLA–PBAT copolymer were synthesized by ring-opening polymerization, as shown in Figure 1, under N_2 atmosphere at 120°C for 4 h. After the reaction, PLLA and PLLA–PBAT copolymer were dried overnight in a vacuum oven at 50°C.

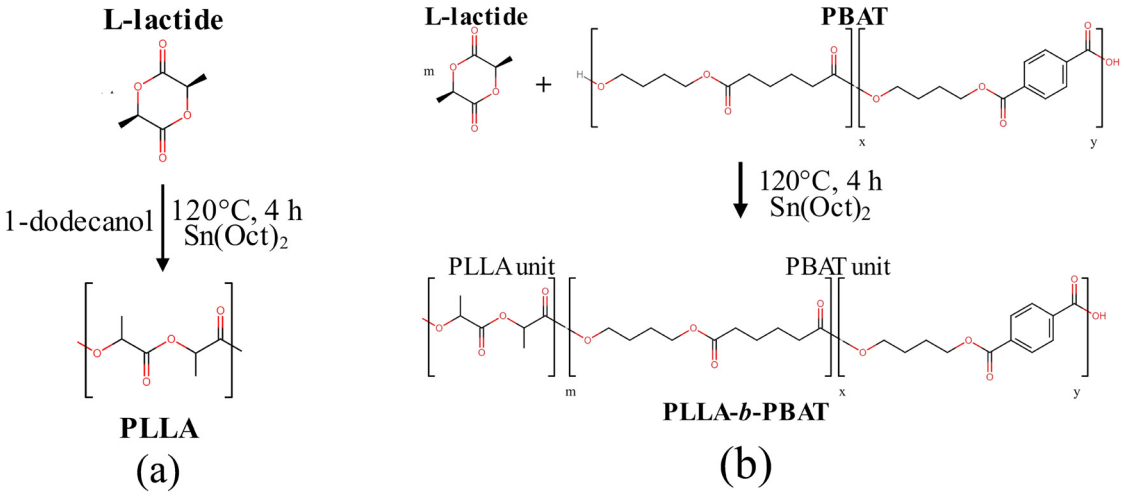

Figure 1: Synthesis of (a) PLLA and (b) PLLA-b-PBAT by ring-opening polymerization.

2.3 Preparation of ST and MWCNT blends

The synthesized PLLA and PLLA–PBAT copolymer were blended with PDLA and MWCNTs (Table 1). PLLA, PLLA–PBAT, and PDLA were dissolved in CH_3Cl (1 g of polymer per 10 mL subjected to magnetic stirring for 3 h at ≅25°C, and then vibrated in an ultrasonic machine for 1 h). After the materials were dissolved, MWCNTs were added to the solution and stirred for another 1 h. The resulting mixed solution was poured onto glass Petri dishes. The films were dried (for 3 days at ≅25°C) to allow the solvent to evaporate. The final film thickness was ≅0.2 mm.

2.4 Characterization

2.4.1 Gel permeation chromatography (GPC)

GPC was used to determine the weight average molecular weight (M_w) and the number average molecular weight (M_n) of the PLLA and PLLA–PBAT copolymer. Approximately, 5 mg of the specimen was dissolved in 3 mL of tetrahydrofuran (THF) and stirred in a water bath (1 h, 50°C). A Waters 2414 refractive index detector was used. The GPC column was eluted using THF at 40°C with a flow rate of 1.0 mL·min^{-1}. The monodispersed polystyrene was used for calibration.

2.4.2 Fourier transform infrared spectroscopy (FTIR)

The chemical structures of polymers and their composites were examined from 400 to 4,000 cm^{-1} using a Perkin-Elmer Frontier FTIR spectrometer (attenuated total reflection [ATR] mode).

2.4.3 Proton nuclear magnetic resonance (^{1}H-NMR)

The functional groups in the PLLA-*b*-PBAT copolymer were determined from ^{1}H-NMR spectra (Bruker Advanced DPX at 300 MHz using $CDCl_3$ solvent at room temperature) and

Table 1: Composition of the prepared films

Sample		PLLA (wt%)	PLLA–PBAT copolymer (wt%)	PDLA (wt%)	MWCNT (phr)
1	PLLA	100	—	—	—
2	PLLA + 5MWCNT	100	—	—	5
3	PLLA–PBAT copolymer	—	100	—	—
4	PLLA–PBAT + 5MWCNT	—	100	—	5
5	ST-PLLA	50	—	50	—
6	ST-PLLA + 5MWCNT	50	—	50	5
7	ST-copolymer	—	50	50	—
8	ST-copolymer + 5MWCNT	—	50	50	5

tetramethyl silane was used as an internal chemical shift standard.

2.4.4 Electrical resistivity

The electrical resistivity of the sample (50 mm × 50 mm × 0.2 mm) was measured using a high resistance meter (Keithley DMM7510) at room temperature.

2.4.5 Mechanical properties

Mechanical properties of film samples were tested using a tensile tester (Texture Analyzer Stable Micro System Model TA.XT Plus) with a cross speed of 2 mm·min^{-1}. The 15 mm × 50 mm sample was cut from the prepared film. The Young's modulus, tensile strength, and elongation at break were measured at 50 ± 5% relative humidity and 25°C. The mean value and standard deviation were computed from five specimens.

2.4.6 Differential scanning calorimetry (DSC)

The thermal properties of the film samples were determined using a DSC (4000 PerkinElmer, USA). The sample (3–5 mg) was placed in an aluminum pan and heated at 10°C·min^{-1} from 25°C to 250°C. The homo-melting temperature ($T_{m,hc}$) and its enthalpy ($\Delta H_{m,hc}$), the ST melting temperature ($T_{m,st}$) and its enthalpy ($\Delta H_{m,st}$), and the glass transition temperature (T_g) were recorded. The total degree of crystallinity (X_c) values for both the homo and ST crystals (X_{st}) were calculated (23):

$$X_c\ (\%) = \frac{\Delta H_{m,hc} + \Delta H_{m,st} - \Delta H_{cc}}{w \times \Delta H^0_{m(blend)}} \times 100\% \quad (1)$$

where $\Delta H_{m,hc}$ and $\Delta H_{m,st}$ are the melting enthalpies of homocrystallites and ST crystallites, respectively; ΔH_{cc} is the cold crystallization enthalpy, and w is the mass fraction of PLLA or the ST in the polymer blend; and $H^0_{m(blend)}$ is the theoretical value of the melting enthalpy for perfect crystals, calculated from

$$H^0_{m(blend)} = H^0_{m,hc} \times f_{hc} + H^0_{m,st} \times f_{st} \quad (2)$$

where $H^0_{m,hc}$ and $H^0_{m,st}$ are the enthalpy values for the homocrystallites (93.6 J·g^{-1}) and the ST crystallites (142 J·g^{-1}), respectively. The f_{hc} and f_{st} are the relative amounts of homo and streocomplex crystallites under non-isothermal conditions and calculated from:

$$f_{hc}\ (\%) = \frac{\Delta H_{m,hc}}{\Delta H_{m,hc} + \Delta H_{m,st}} \times 100\% \quad (3)$$

$$f_{st}\ (\%) = \frac{\Delta H_{m,st}}{\Delta H_{m,hc} + \Delta H_{m,st}} \times 100\% \quad (4)$$

where $\Delta H_{m,hc}$ and $\Delta H_{m,st}$ were obtained from the thermograms as in Eq. 1. The crystallinity of ST crystallites, X_{st}, was then calculated from Eq. 5:

$$X_{st}\ (\%) = X_c \times f_{st} \times 100\% \quad (5)$$

2.4.7 Scanning electron microscopy (SEM)

The morphology of fractured surfaces was examined using an SEM technique (TM4000Plus Tabletop Microscope, HITACHI) at 10 kV. The sample was fractured in liquid nitrogen and sputter-coated with a 20 nm Au layer prior to examination.

2.4.8 Thermogravimetric analysis (TGA)

TGA was performed using a PerkinElmer TGA 4000. The sample (10–15 mg) was heated from 30°C to 600°C with a heating rate of 20°C·min^{-1} under a N_2 flow rate of 20 mL·min^{-1}. The weight loss was recorded and normalized against the initial weight. The thermal degradation temperature was specified from the decomposition temperature at 10% weight loss.

3 Results and discussion

3.1 Chemical structure

The GPC results show that the synthesized PLLA had $M_w \cong 70{,}932$ g·mol^{-1} and $M_n \cong 32{,}519$ g·mol^{-1}. The PLLA–PBAT copolymer had $M_w \cong 70{,}932$ g·mol^{-1} and $M_n \cong 38{,}853$ g·mol^{-1}. Figure 2(a) shows the FTIR spectra from 500 to 4,000 cm^{-1} of the synthesized PLLA, the PLLA–PBAT copolymer, and their ST and composites. PLLA shows two peaks at 2,995 and 2,948 cm^{-1}, corresponding to asymmetric and symmetric –CH stretching, respectively. Additionally, PLLA was successfully synthesized *via* ring-opening polymerization in the presence of C═O stretching at 1,752 cm^{-1} (24). The peaks at 2,960 and 2,873 cm^{-1} in the FTIR spectrum of PBAT correspond to the asymmetric and symmetric stretching vibrations of the CH_2 groups, respectively. These peaks are indicative of the aliphatic segments present in the PBAT polymer structure. The presence of a strongly convoluted (–C ═ O) absorption band at 1,741 cm^{-1} in the infrared (IR) spectrum of PBAT suggests that there are multiple types of carbonyl groups (25). The peak at 729 cm^{-1} in the PBAT IR

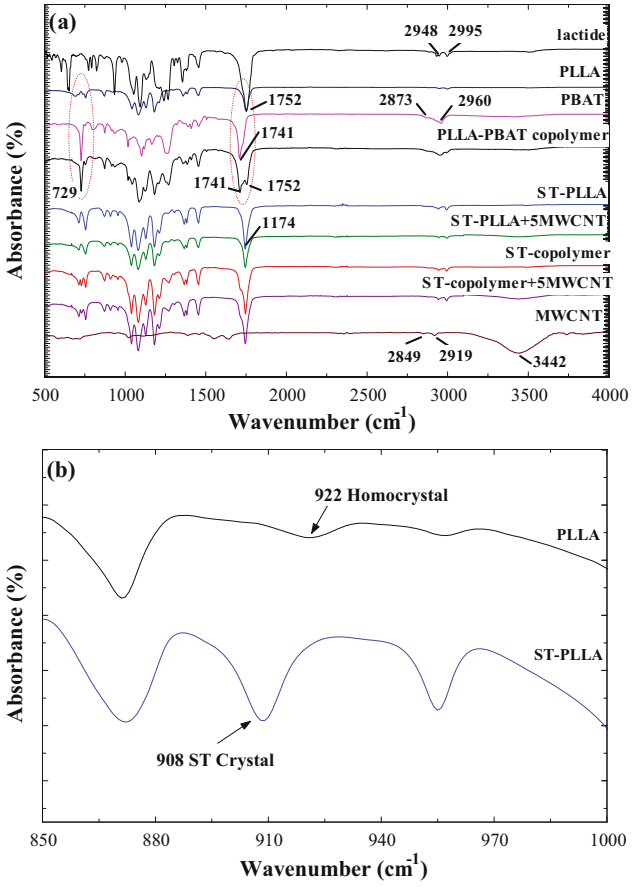

Figure 2: FTIR spectra of (a) PLLA, PLLA–PBAT copolymer, ST polymers, and polymer/MWCNT composites and (b) the expanded region from 850 to 1,000 cm^{-1} of PLLA and ST-PLLA.

spectrum indicates the presence of out-of-plane bending vibrations of the phenylene rings, confirming the contribution of aromatic terephthalate units to the polymer's structure (26).

The FTIR spectra of the PLLA–PBAT copolymer exhibit only strong peaks at 1,714 and 1,752 cm^{-1}, corresponding to the ester group (–C═O) stretching vibrations of the interaction between PLLA and PBAT (27). Malinowski et al. (28) also reported that the FTIR spectrum of the PLLA–PBAT copolymer shows the CH-plane benzene ring vibration at 729 cm^{-1}, which is absent in pure PLLA (29). This result confirmed that the synthesis conditions and the initiator generated the PLLA–PBAT copolymer *via* ring-opening polymerization.

Then, we blended the PLLA and PLLA–PBAT copolymer with PDLA to create the ST structure. The FTIR spectra of ST samples show peaks at similar positions to those of pure PLLA and PLLA–PBAT copolymer. However, the FTIR peak shifted from 922 to 908 cm^{-1} for the ST formation (Figure 2b). The 922 cm^{-1} band is assigned to the PLLA homocrystallite (30), whereas the peak at 908 cm^{-1} corresponds to the ST crystallite (31). Moreover, in the ST sample, the carbonyl (C═O) stretching was observed at 1,744 cm^{-1}.

In addition, the polymer/MWCNT composite samples showed intense bands near 3,442 cm^{-1}, equivalent to the OH carboxyl group stretching vibrations. The 2,992–2,888 cm^{-1} band corresponds to the C–H bond symmetric stretching in carbonaceous material and the 1,641–1,548 cm^{-1} range is assigned to the C═O bond (32). Moreover, the copolymers with MWCNTs had no other new peaks (32); thus, blending MWCNTs into the copolymer did not lead to significant chemical interactions, i.e., any change in the nanocomposite properties resulted from physical interactions alone.

The ^{1}H-NMR spectra of PLLA, PBAT, and PLLA–PBAT copolymer are shown in Figure 3. The spectrum of pure PLLA shows signals at 5.16 (peak 1) and 1.56 (peak 2) corresponding to the methine proton (CH) and methyl proton (CH_3) of the lactic acid units (33). For PBAT, the signals at the signal of aromatic protons appearing at 8.09 ppm (peak 6) indicate the phenylene structure of the CH in the benzene ring, and 2.34 ppm (peak 3) and 1.67–1.69 ppm (peak 8) were assigned to the outer and inner CH_2 groups, respectively. In the BT unit, the outer and inner methylene protons were observed at 4.38–4.46 ppm (peak 5) and 1.66 ppm (peak 8), respectively. For the BA unit, the CH_2 groups in adipic acid appear at 4.11–4.17 ppm (peak 4), 2.34 ppm (peak 3), and 1.69 ppm (8). Additionally, the methylene protons of the butanediol units close to the terminal −OH of the macroinitiator were assigned to 3.65–3.75 ppm (peak 10) (34). However, after the ROP of the PLLA–PBAT copolymer, the 3.67–3.75 ppm peak vanished entirely in the spectrum of PLLA-*b*-PBAT, and the PLLA-related new proton signals were also observed at 5.09 and 1.49 ppm (22,35). This showed

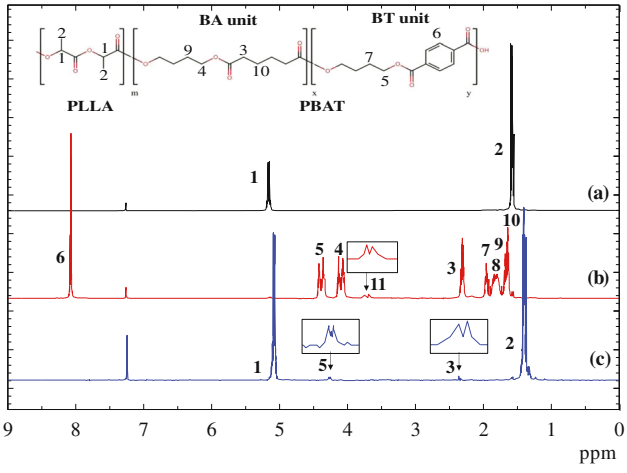

Figure 3: ^{1}H-NMR spectra of (a) PLLA, (b) PBAT, and (c) the PLLA–PBAT copolymer.

that the hydroxyl groups of PBAT had started the L-lactide in the ring-opening polymerization, showing that the PLLA–PBAT structure had been formed.

3.2 Electrical properties

Figure 4 shows the electrical resistivity plot of polymer/MWCNT composite films. The materials without MWCNTs did not conduct electricity, and they were effective insulators (36). The composites showed a significant increase in conductivity with the addition of 5 phr of MWCNTs. Notably, the composite with 5 phr of MWCNTs had a surface electrical resistance of $\cong 10^6$ Ω, similar to those of films used in the ESD application in the range of 10^6–10^9 Ω (37). Note that 5 phr of MWCNTs had the lowest content, which induced the electrical conductivity of polymer composites for ESD use. When >5 phr of MWCNTs were added to the system, the composite film could not be formed. These results demonstrated that the electrical resistivity of the films and a higher content of MWCNTs resulted in lower electrical resistivity (higher conductivity). In the case of copolymer/MWCNT blends, the resistivity of the polymer with MWCNTs at 5 phr was similar, which means that the polymer type does not affect the electrical properties of the composite.

3.3 Tensile properties

Tensile tests were performed on the film specimens of PLLA, PLLA–PBAT copolymer, ST-PLLA, ST-copolymer, and their composites with MWCNTs. Figure 5(a)–(c) shows the tensile strength, modulus of elasticity, and elongation at the break of the tested samples, respectively.

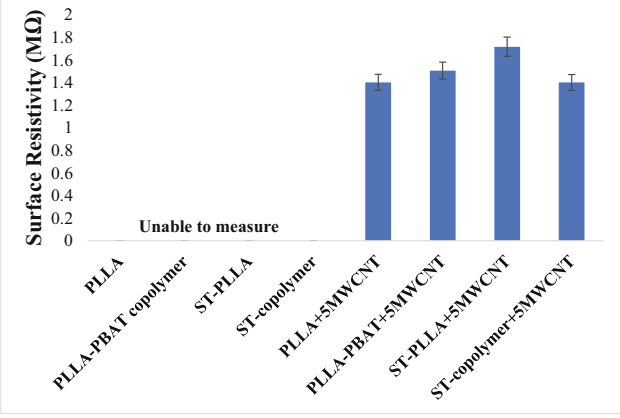

Figure 4: Surface resistivity of various polymers and their MWCNT composites.

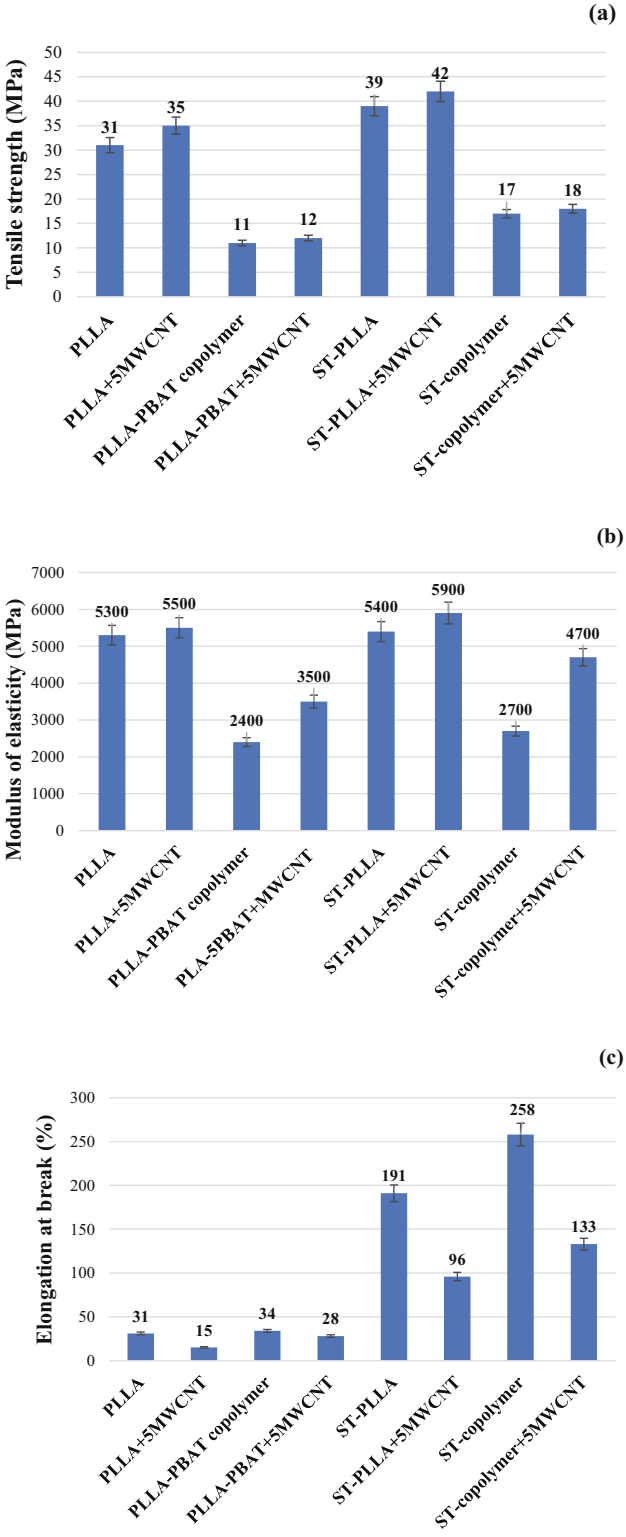

Figure 5: Tensile properties of as-prepared films: (a) tensile strength, (b) modulus of elasticity, and (c) elongation at break.

PLLA had a lower tensile strength of 31 MPa, Young's modulus of 5,300 MPa, and an elongation at break of 31% compared to those of ST-PLLA (39 MPa, 5,400 MPa, and 191%). The mechanical properties of ST PLLA were higher than those of PLLA due to increased bonding between PLLA and PLDA. This result was consistent with that of Tsuji et al. (38) stating that the mechanical properties of ST PLLA films were superior to those of PLLA films. The micro-phase structure difference was generated in the ST of PLLA as a result of dense chain packing in the amorphous region (strong interaction between L- and D-units). Meanwhile, the PLLA–PBAT copolymer showed an increase in elongation but a decrease in strength and modulus. The tensile strength of PLLA was almost 60% higher than that of the PLLA–PBAT copolymer because of the higher flexibility of PBAT. Ming et al. (39) investigated the reaction occurring between PLLA and PBAT during blending. The formation of the PLLA–PBAT copolymer improved compatibility, which increased the chain extension of PLLA and PBAT. The addition of MWCNTs into all samples showed an increase in tensile strength and modulus (≅10%) along with a slightly lower elongation at break. Andrews and Weisenberger (40) reported that as MWCNT increased, elongation at break decreased, leading to lower ductility in the polymer matrix. The as-prepared composite samples showed decreased elongation at break, according to the high stiffness behavior of MWCNTs, indicating the decrease in ductility of polymer/MWCNT composites. The decrease in elongation at break was also attributed to the partially miscible dispersion of nanotubes in the polymer matrix (41). This will be covered in more detail in the section on morphological analysis.

3.4 Thermal properties

Figure 6(a) and (b) shows the first heating thermograms of the film samples. The T_g, T_m, and % X_c of each specimen are recorded in Table 2. As shown in Figure 5(a), the PLLA has two thermal steps: (1) a T_g ≅ 47°C and (2) an endothermic fusion step (T_m) with a maximum at ≅170°C. The T_g and T_m of the PLLA–PBAT copolymer decreased to ≅45°C and ≅165°C, respectively, compared to the PLLA homopolymer. This might be attributed to the formation of hydrogen bonds between the polymer chains, which gradually enhanced molecular flexibility. Moreover, the molecular chains of PLLA were widened by PBAT, resulting in the reduction of applied energy for molecular motion (42). The addition of MWCNTs caused a slight increase in T_g, T_m, and % X_c of PLLA and PLLA–PBAT copolymer because of the reinforcing and nucleating effects of nanotubes on both polymers.

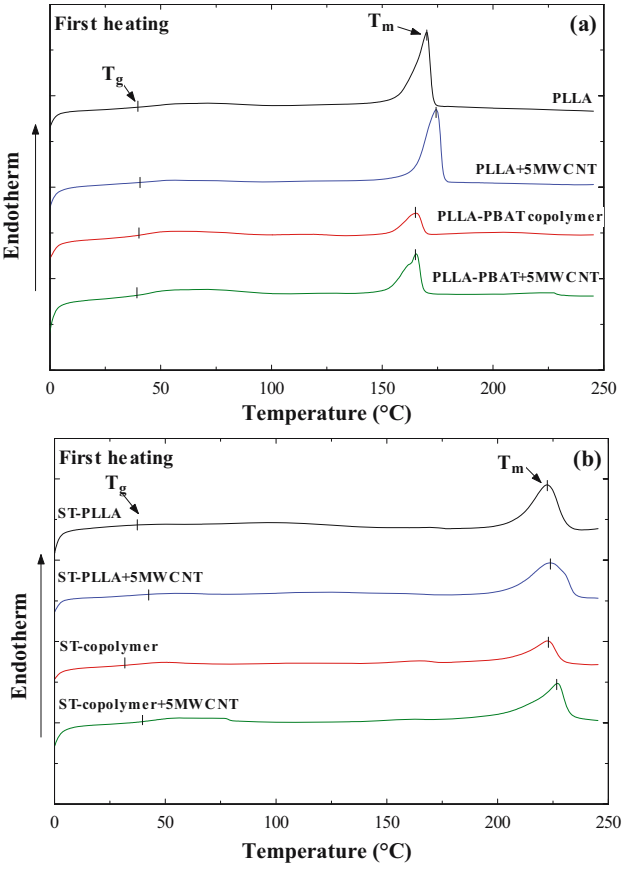

Figure 6: First heating thermograms of (a) PLLA, PLLA–PBAT copolymer, and their composites with MWCNTs and (b) ST-PLLA, ST-copolymer, and their composites with MWCNTs.

In addition, the DSC results of ST samples are shown in Figure 6(b). A complete formation of ST crystallites (no homocrystallites) was obtained for all samples with a melting peak at ≅222–223°C, higher than that of PLLA ≅50°C (43). The T_m, T_g, and % X_{st} of ST-PLLA were ≅222°C, 47°C, and 34%, respectively (Table 2). The T_g and % X_{st} of ST-copolymer decreased to ≅40°C and 17%, respectively, while the T_m was unchanged at ≅222°C compared to those of ST-PLLA. Moreover, the T_g, T_m, and % X_{st} of ST-PLLA and ST-copolymer increased in the presence of MWCNTs. The nanofillers might entail a higher concentration of the nucleating agent, promoting the formation of more crystallization nuclei and increasing the degree of crystallization. The DSC profiles exhibited that MWCNTs serve as nucleating agents in polymer nanocomposites (44).

3.5 X-ray diffraction (XRD) analysis

Figure 7(a) and (b) depicts XRD spectra of as-synthesized samples and their composites. The pure PLLA, PLLA–PBAT

Table 2: Thermal properties and crystallinities of the prepared samples from the first heating thermograms

Sample	T_g (°C)	Melting 1		Melting 2		% X_c	% X_{st}
		$T_{m,hc}$ (°C)	$\Delta H_{m,hc}$ (J·g^{-1})	$T_{m,ST}$ (°C)	$\Delta H_{m,ST}$ (J·g^{-1})		
PLLA	47.2	170.0	41.8	—	—	44.6	—
PLLA + 5MWCNT	47.8	174.4	42.4	—	—	45.3	—
PLLA–PBAT copolymer	45.6	165.1	13.5	—	—	14.4	—
PLLA–PBAT + 5MWCNT	46.2	166.2	22.9	—	—	24.5	—
ST–PLLA	47.2	—	—	222.6	48.3	—	34.0
ST–PLLA + 5MWCNT	48.1	—	—	223.6	50.1	—	35.3
ST–copolymer	40.5	—	—	222.4	25.1	—	17.7
ST–copolymer + 5MWCNT	43.7	—	—	227.1	45.5	—	32.0

copolymer, and their composites (Figure 7a) showed two major characteristic peaks at 16.7° and 18.8°, corresponding to the homocrystal peaks of PLLA (45). Figure 7(b) shows the XRD peaks of ST-PLLA and ST-copolymer at 11.6°, 20.6°, and 23.5°, in good accordance with the previous studies (46,47). These peaks correspond to ST crystallites being formed in a triclinic unit cell, in which PLLA and PDLA segments are packed in parallel in a helical conformation (48). The PLLA–PBAT copolymer and ST-copolymer crystallization peaks were smaller than PLLA and ST-PLLA due to PBAT hindering crystallization and lowering final crystallinity. On the other hand, the crystallinity of composite samples increased, confirming that MWCNTs contributed to the production of more crystallization nuclei. This result corresponds to the DSC analysis (Section 3.4).

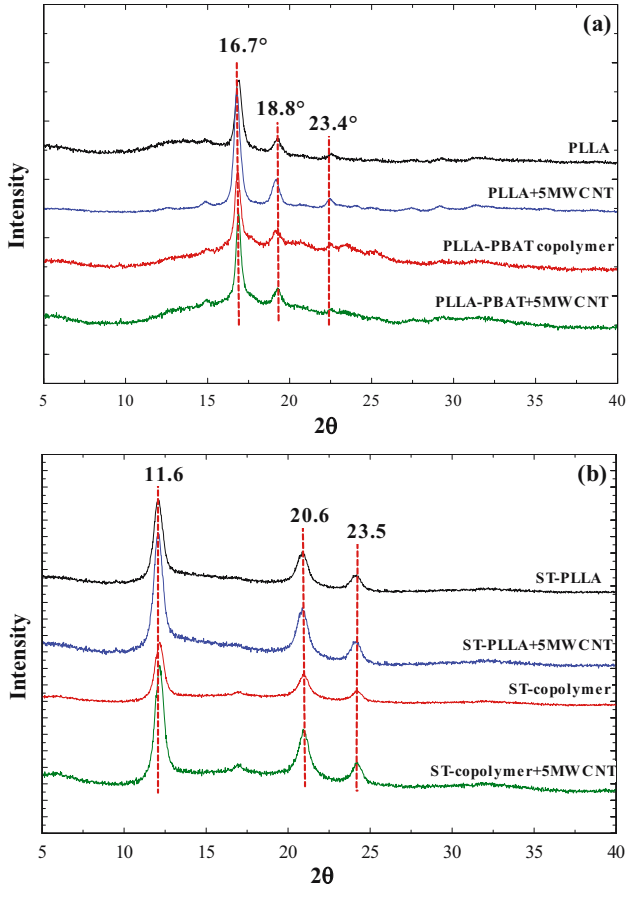

Figure 7: XRD profiles of (a) PLLA, PLLA–PBAT copolymer, and their composites with MWCNTs. (b) ST-PLLA, ST-copolymer, and their composites with MWCNTs.

3.6 Morphology

The SEM images of the fractured surfaces are shown in Figure 8(a)–(h). The PLLA and ST-PLLA had smooth and homogeneous fractured surfaces (Figure 8a and e). They formed a good continuous phase in a miscible PLLA and PDLA blend. This led to a typical brittle fracture, consistent with the previous report (31). In contrast, PLLA–PBAT copolymer and ST-copolymer (Figure 8c and g) showed rougher surfaces and more ductile behavior than the pure PLLA and ST-PLLA. This demonstrated that the PLLA toughness was improved by the PBAT copolymer. Similar to the study of Srithep et al. (33), the cross-sectional surface of the PLLA copolymer was rougher, implying that the local ductile was generated during the fracture. This indicated that the copolymer efficiently improved the interfacial adhesion of PLLA. Moreover, for samples with MWCNTs (Figure 8b, d, f, and h), the nanotubes were partially dispersed in the polymer matrix due to the strong van der Waals interaction (49). In the case of the observed dispersion, it seems that the MWCNTs are not uniformly distributed throughout the polymer matrix, as the processing conditions can influence the dispersion outcome (50). Therefore, the aggregation of MWCNTs was also observed in the polymer matrix. This poor dispersion can result in a range of negative effects. This may reduce the mechanical properties and hinder the desired electrical and thermal conductivity properties of polymer/MWCNT composites.

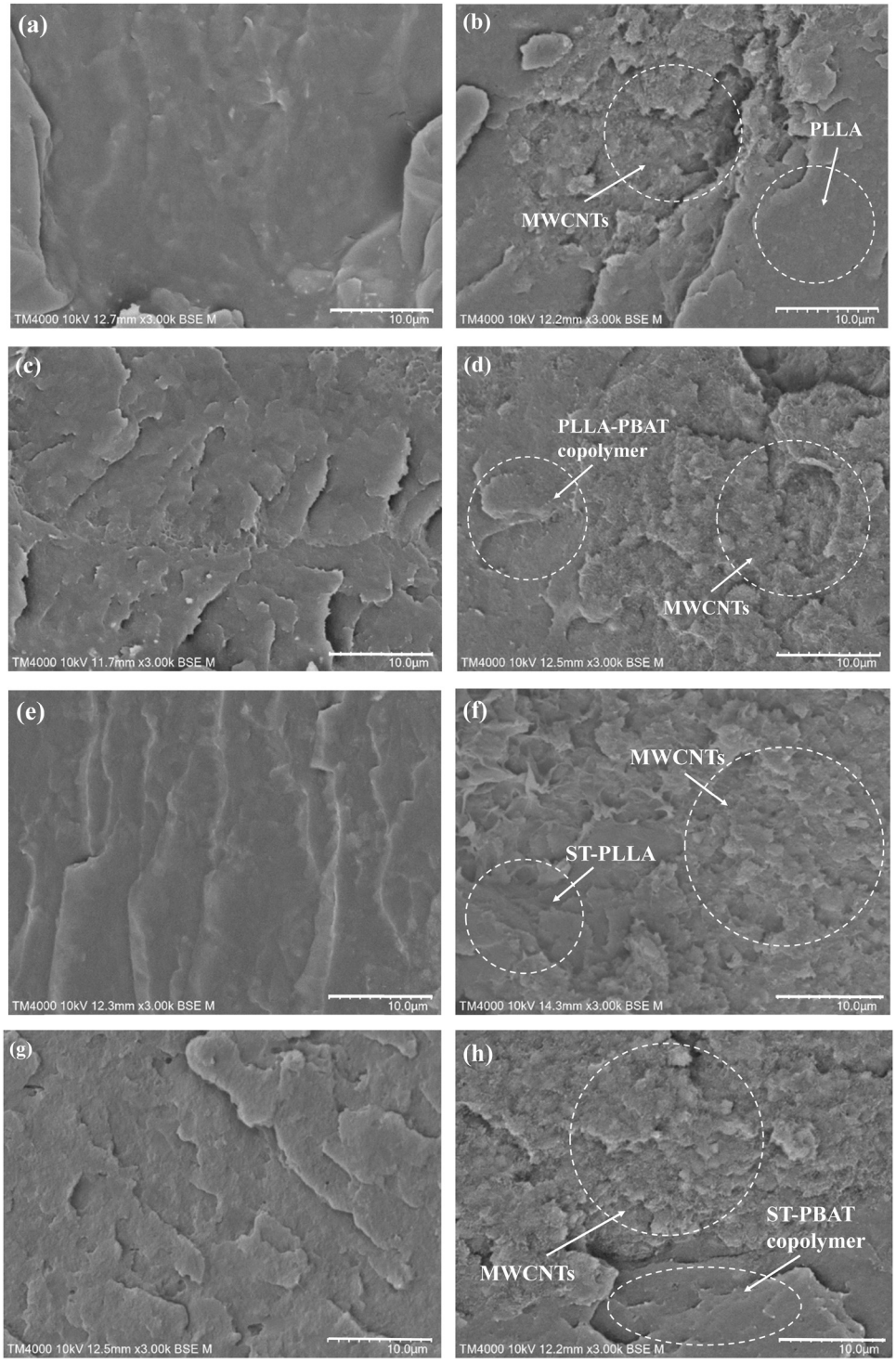

Figure 8: SEM micrographs of fractured surfaces of (a) PLLA, (b) PLLA + MWCNT, (c) PLLA–PBAT copolymer, (d) PLLA–PBAT copolymer + MWCNT, (e) ST-PLLA, (f) ST-PLLA + MWCNT, (g) ST-copolymer, and (h) ST-copolymer + MWCNT.

3.7 Thermal stability

The thermal stability of PLLA, PLLA–PBAT copolymer, ST-PLLA, and ST-copolymer with and without MWCNTs was determined from 30°C to 600°C by TGA. The results are shown in Figure 9(a) and (b).

The thermal degradation of neat PLLA and the PLLA/MWCNT composite occurred in one single step.

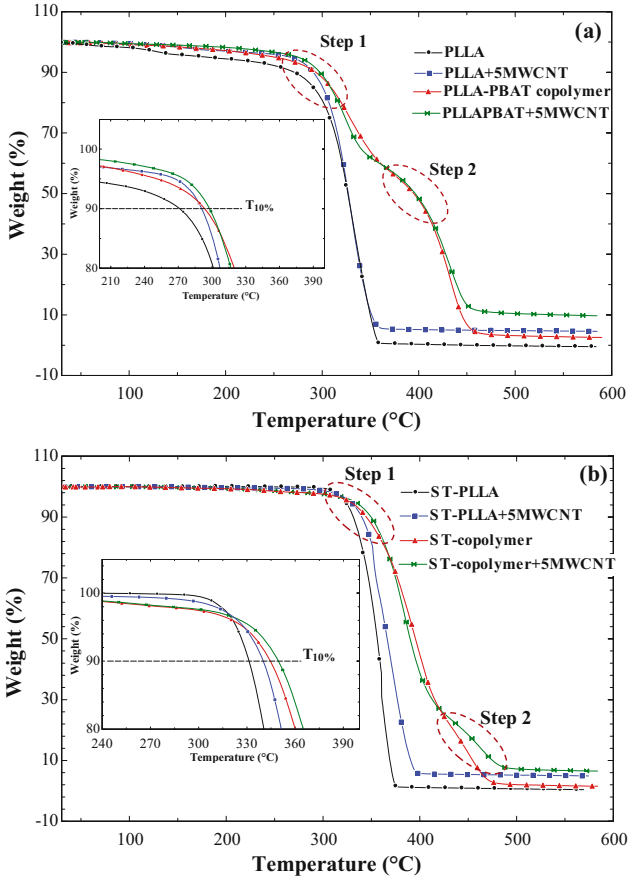

Figure 9: TGA thermograms of (a) PLLA, PLLA–PBAT copolymer, and their composites and (b) ST-PLLA, ST-copolymer, and their composites.

PLLA had a $T_{10\%}$ of 278.2°C while the PLLA/MWCNT composite had a $T_{10\%}$ of 292.8°C, indicating a higher thermal stability of the composite. Moreover, the PLLA–PBAT copolymer and its composite showed two degradation steps (Figure 9a). For the PLLA–PBAT copolymer, PLLA began to degrade at ≅290°C (step 1), whereas PBAT degraded at ≅400°C (step 2), corresponding to the different thermal degradation temperatures of the PLLA and PBAT phases (51). The thermal stability of the copolymer/MWCNT composite increased, showing the MWCNTs strengthened the thermal stability of the copolymer (52).

As shown in Figure 9(b), the ST-PLLA slowly degraded with higher thermal stability (≅20%) than that of the neat PLLA. The thermal degradation of the ST sample was improved because the molecular mobility was significantly reduced as a result of the strong interaction between the PLLA and PDLA chains (53). The ST-copolymer and its composite exhibited two degradation steps at ≅350°C (step 1) and ≅430°C (step 2). The $T_{10\%}$ of ST-PLLA and ST-copolymer composites were 345.0°C and 347.6°C, respectively, which were higher than those of ST-PLLA (343.9°C) and ST-copolymer (345.3°C). This result showed that the addition of MWCNTs to ST-PLLA and ST-copolymer led to their higher thermal stability (49). Moreover, composite samples had a significant increase in the residual mass since MWCNTs decompose at a temperature higher than 600°C (54)

4 Conclusions

PLLA and PLLA–PBAT copolymer were successfully synthesized by ring-opening polymerization of lactides, using 1-dodecanol and PBAT as initiators, respectively. Stannous octoate was used as a catalyst for the synthesis of both polymers. The ST films of PLLA and PLLA–PBAT copolymer were prepared by the addition of 50 wt% PDLA using the solution casting method. Moreover, the as-prepared polymer/MWCNT composite films were obtained *via* the solution casting process as well. The toughness of PLLA was improved by copolymerization with PBAT, according to the enhancement of elongation at break. Based on the DSC results, the ST formation assisted in increasing the melting temperature of PLLA and its copolymer by ≅50°C. Furthermore, the homo-crystals of PLLA and the copolymer were completely converted into ST crystals. FT-IR results demonstrated that the chemical structure of polymers was unchanged with the addition of MWCNTs. However, the tensile strength and modulus of polymer/MWCNT composites significantly improved along with the reduction of elongation at break. The nanofillers caused an increase in the crystallinity and thermal degradation of the polymer/MWCNT composites. The surface resistance of the ST-copolymer with 5 phr of MWCNTs was about ≅10^6 Ω, suitable for ESD applications. These findings provided a foundation for further investigation into novel, multifunctional biodegradable polymer composites with the potential for use in ESD applications. The final properties of polymer nanocomposites could be improved by applying suitable compatibilizers or dispersing agents or a high-shear-mixing process to enhance the distribution of nanofillers.

Acknowledgements: The authors thank the Faculty of Engineering, Mahasarakham University, Faculty of Science and Technology, Rajabhat Maha Sarakham University, and National Metal and Materials Technology Center (MTEC), National Science and Technology Development Agency (NSTDA) for providing the research and testing facilities.

Funding information: This research received funding support from the NSTDA under the TGIST project (contract number: SCA-CO-2563-12084-TH).

Author contributions: Onpreeya Veang-in: writing – original draft, methodology, experimental data acquisition; Yottha Srithep: writing – review and editing, instructional support, resources, project administration; John Morris: writing – review and editing; Darunee Aussawasathien: writing – review and editing, methodology, formal analysis; Patnarin Worajittiphon: writing – review and editing.

Conflict of interest: The authors state no conflict of interest.

References

(1) Sarul DS, Arslan D, Vatansever E, Kahraman Y, Durmus A, Salehiyan R, et al. Preparation and characterization of PLA/PBAT/CNC blend nanocomposites. Colloid Polym Sci. 2021;299(6):987–98. doi: 10.1007/s00396-021-04822-9.

(2) Nofar M, Park CB. Poly (lactic acid) foaming. Prog Polym Sci. 2014;39(10):1721–41. doi: 10.1016/j.progpolymsci.2014.04.001.

(3) Feng L, Bian X, Li G, Chen Z, Chen X. Compatibility, mechanical properties and stability of blends of polylactide and polyurethane based on poly (ethylene glycol)-b-polylactide copolymers by chain extension with diisocyanate. Polym Degrad Stab. 2016;125:148–55. doi: 10.1016/j.polymdegradstab.2015.12.017.

(4) Sun Q, Mekonnen T, Misra M, Mohanty AK. Novel biodegradable cast film from carbon dioxide based copolymer and poly (lactic acid). J Polym Env. 2016;24(1):23–36. doi: 10.1007/s10924-015-0743-6.

(5) Flodberg G, Helland I, Thomsson L, Fredriksen SB. Barrier properties of polypropylene carbonate and poly (lactic acid) cast films. Eur Polym J. 2015;63:217–26. doi: 10.1016/j.eurpolymj.2014.12.020.

(6) Phetwarotai W, Tanrattanakul V, Phusunti N. Mechanical characteristics and thermal behaviours of polylactide blend films: influence of nucleating agent and poly (butylenes adipate-co-terephthalate). Plast. 2016;45(8):333–45. doi: 10.1080/14658011.2016.1197556.

(7) Shi N, Dou Q. Non-isothermal cold crystallization kinetics of poly (lactic acid)/poly (butylene adipate-co-terephthalate)/treated calcium carbonate composites. J Therm Anal Calorim. 2015;119(1):635–42. doi: 10.1007/s00289-009-0047-x.

(8) Zhang C, Lan Q, Zhai T, Nie S, Luo J, Yan W. Melt crystallization behavior and crystalline morphology of polylactide/poly (ε-caprolactone) blends compatibilized by lactide-caprolactone copolymer. Polymers. 2018;10(11):1181. doi: 10.3390/polym10111181.

(9) Bhatia A, Gupta R, Bhattacharya S, Choi H. Compatibility of biodegradable poly (lactic acid)(PLA) and poly (butylene succinate)(PBS) blends for packaging application. Korea Aust Rheol J. 2007;19(3):125–31.

(10) Sun Z, Zhang B, Bian X, Feng L, Zhang H, Duan R, et al. Synergistic effect of PLA–PBAT–PLA tri-block copolymers with two molecular weights as compatibilizers on the mechanical and rheological properties of PLA/PBAT blends. RSC Adv. 2015;5(90):73842–9. doi: 10.1039/c5ra11019j.

(11) Na Y-H, He Y, Shuai X, Kikkawa Y, Doi Y, Inoue Y. Compatibilization effect of poly (ε-caprolactone)-b-poly (ethylene glycol) block copolymers and phase morphology analysis in immiscible poly (lactide)/poly (ε-caprolactone) blends. Biomacromolecules. 2002;3(6):1179–86. doi: 10.1021/bm020050r.

(12) Srithep Y, Pholharn D, Turng L-S, Veang-in O. Injection molding and characterization of polylactide stereocomplex. Polym Degrad Stab. 2015;120:290–9. doi: 10.1016/j.polymdegradstab.2015.07.017.

(13) Jiang L, Shen T, Xu P, Zhao X, Li X, Dong W, et al. Crystallization modification of poly (lactide) by using nucleating agents and stereocomplexation. E-Polym. 2016;16(1):1–13. doi: 10.1515/epoly-2015-0179.

(14) Srisuwan Y, Baimark Y. Controlling stereocomplexation, heat resistance and mechanical properties of stereocomplex polylactide films by using mixtures of low and high molecular weight poly (D-lactide) s. E-Polym. 2018;18(6):485–90. doi: 10.1515/epoly-2018-0115.

(15) Chen J, Rong C, Lin T, Chen Y, Wu J, You J, et al. Stable co-continuous PLA/PBAT Blends compatibilized by interfacial stereocomplex crystallites: Toward full biodegradable polymer blends with simultaneously enhanced mechanical properties and crystallization rates. Macromol. 2021;54(6):2852–61. doi: 10.1021/acs.macromol.0c02861.

(16) Ibrahim KS. Carbon nanotubes-properties and applications: a review. Carbon Lett. 2013;14(3):131–44. doi: 10.5714/CL.2013.14.3.131.

(17) Coleman JN, Khan U, Blau WJ, Gun'ko YK. Small but strong: a review of the mechanical properties of carbon nanotube–polymer composites. Carbon. 2006;44(9):1624–52. doi: 10.1016/j.carbon.2006.02.038.

(18) Moisala A, Li Q, Kinloch I, Windle A. Thermal and electrical conductivity of single-and multi-walled carbon nanotube-epoxy composites. Compos Sci Technol. 2006;66(10):1285–8. doi: 10.1016/j.compscitech.2005.10.016.

(19) Hu Y, Shenderova OA, Hu Z, Padgett CW, Brenner DW. Carbon nanostructures for advanced composites. Rep Prog Phys. 2006;69(6):1847. doi: 10.1088/0034-4885/69/6/R05.

(20) Spitalsky Z, Tasis D, Papagelis K, Galiotis C. Carbon nanotube–polymer composites: Chemistry, processing, mechanical and electrical properties. Prog Polym Sci. 2010;35(3):357–401. doi: 10.1016/j.progpolymsci.2009.09.003.

(21) Ramontja J, Ray SS, Pillai SK, Luyt AS. High-performance carbon nanotube-reinforced bioplastic. Macromol Mater Eng. 2009;294(12):839–46. doi: 10.1002/mame.200900197.

(22) Pholharn D, Srithep Y. Optimization of poly (L-lactide)-polybutylene adipate terephthalate diblockcopolymer by ring opening polymerization. IOP Conf Ser Mater Sci Eng. 2019;526:012026. doi: 10.1088/1757-899X/526/1/012026.

(23) Sarasua JR, Arraiza AL, Balerdi P, Maiza I. Crystallinity and mechanical properties of optically pure polylactides and their blends. Polym Eng Sci. 2005;45(5):745–53. doi: 10.1002/pen.20331.

(24) Pholharn D, Srithep Y, Morris J. Effect of initiators on synthesis of poly (L-lactide) by ring opening polymerization. IOP Conf Ser Mater Sci Eng. 2017;213:012022. doi: 10.1088/1757-899X/213/1/012022.

(25) Hexig A, Hexig B. Characterization of compositional gradient structure of polymeric materials by FTIR technology. infrared spectroscopy-materials. Science, Engineering and Technology. Rijeka, Croatia: IntechOpen; 2012. p. 339–52.

(26) Tavares L, Ito N, Salvadori M, Dos Santos D, Rosa D. PBAT/kraft lignin blend in flexible laminated food packaging: Peeling resistance and thermal degradability. Polym Test. 2018;67:169–76. doi: 10.1016/j.polymertesting.2018.03.004.

(27) Wu D, Huang A, Fan J, Xu R, Liu P, Li G, et al. Effect of blending procedures and reactive compatibilizers on the properties of biodegradable poly (butylene adipate-co-terephthalate)/poly (lactic acid) blends. J Polym Eng. 2021;41(2):95–108. doi: 10.1515/polyeng-2020-0161.
(28) Malinowski R, Moraczewski K, Raszkowska-Kaczor A. Studies on the uncrosslinked fraction of PLA/PBAT blends modified by electron radiation. Mater. 2020;13(5):1068. doi: 10.3390/ma13051068.
(29) Kilic NT, Can BN, Kodal M, Ozkoc G. Compatibilization of PLA/PBAT blends by using Epoxy-POSS. J Appl Polym Sci. 2019;136(12):47217. doi: 10.1002/app.47217.
(30) Srithep Y, Pholharn D. Plasticizer effect on melt blending of polylactide stereocomplex. E-Polym. 2017;17(5):409–16. doi: 10.1515/epoly-2016-0331.
(31) Veang-in O, Srithep Y, Morris J, Pholharn D. Characterization of polymer composites between stereocomplex polylactide blends with poly (methyl methacrylate. J Mater Sci. 2021;28(4):474–81. doi: 10.5755/j02.ms.30315.
(32) Ahmad AF, Aziz SA, Obaiys SJ, Zaid MHM, Matori KA, Samikannu K, et al. Biodegradable poly (lactic acid)/poly (ethylene glycol) reinforced multi-walled carbon nanotube nanocomposite fabrication, characterization, properties, and applications. Polym J. 2020;12(2):427. doi: 10.3390/polym12020427.
(33) Srithep Y, Veang-In O, Pholharn D, Turng L-S, Morris J. Improving polylactide toughness by plasticizing with low molecular weight polylactide-poly (Butylene Succinate) copolymer. J Renew Mater. 2021;9(7):1267. doi: 10.32604/jrm.2021.015604.
(34) Zhao P, Liu W, Wu Q, Ren J. Preparation, mechanical, and thermal properties of biodegradable polyesters/poly (lactic acid) blends. J Nanomater. 2010;2010:1–6. doi: 10.1155/2010/287082.
(35) Ding Y, Lu B, Wang P, Wang G, Ji J. PLA-PBAT-PLA tri-block copolymers: Effective compatibilizers for promotion of the mechanical and rheological properties of PLA/PBAT blends. Polym Degrad Stab. 2018;147:41–8. doi: 10.1016/j.polymdegradstab.2017.11.012.
(36) Ke K, McMaster M, Christopherson W, Singer KD, Manas-Zloczower I. Highly sensitive capacitive pressure sensors based on elastomer composites with carbon filler hybrids. Compos Part A Appl Sci Manuf. 2019;126:105614. doi: 10.1016/j.compositesa.2019.105614.
(37) Singh SP, El-Khateeb H. Evaluation of a proposed test method to measure surface and volume resistance of static dissipative packaging materials. Packag Technol Sci. 1994;7(6):283–9. doi: 10.1002/pts.2770070605.
(38) Tsuji H, Hyon SH, Ikada Y. Stereocomplex formation between enantiomeric poly(lactic acid)s. 3. Calorimetric studies on blend films cast from dilute solution. Macromolecules. 1991;24(20):5651–6. doi: 10.1021/ma00020a026.
(39) Ming M, Zhou Y, Wang L, Zhou F, Zhang Y. Effect of polycarbodiimide on the structure and mechanical properties of PLA/PBAT blends. J Polym Res. 2022;29(9):371. doi: 10.1007/s10965-022-03227-8.
(40) Andrews R, Weisenberger M. Carbon nanotube polymer composites. Curr Opin Solid State Mater Sci. 2004;8(1):31–7. doi: 10.1016/j.cossms.2003.10.006.
(41) Mat Desa MSZ, Hassan A, Arsad A, Arjmandi R, Mohammad NNB. Influence of rubber content on mechanical, thermal, and morphological behavior of natural rubber toughened poly (lactic acid)–multiwalled carbon nanotube nanocomposites. J Appl Polym Sci. 2016;133(48):1–9. doi: 10.1002/app.44344.
(42) Shinyama K. Mechanical and electrical properties of polylactic acid with aliphatic-aromatic polyester. J Eng Sci. 2018;2018:1–7. doi: 10.1155/2018/6597183.
(43) Ikada Y, Jamshidi K, Tsuji H, Hyon SH. Stereocomplex formation between enantiomeric poly (lactides). Macromolecules. 1987;20(4):904–6. doi: 10.1021/ma00170a034.
(44) Ceregatti T, Pecharki P, Pachekoski WM, Becker D, Dalmolin C. Electrical and thermal properties of PLA/CNT composite films. Rev Mater. 2017;22(3). doi: 10.1590/S1517-707620170003.0197.
(45) Li L, Song G, Tang G. Novel biodegradable polylactide/poly (butylene succinate) composites via cross-linking with methylene diphenyl diisocyanate. Polym Plast Technol Eng. 2013;52(12):1183–7. doi: 10.1080/03602559.2013.798817.
(46) Shao J, Xiang S, Bian X, Sun J, Li G, Chen X. Remarkable melting behavior of PLA stereocomplex in linear PLLA/PDLA blends. Ind Eng Chem Res. 2015;54(7):2246–53. doi: 10.1021/ie504484b.
(47) Tsuji H. Poly (lactide) stereocomplexes: Formation, structure, properties, degradation, and applications. Macromol Biosci. 2005;5(7):569–97. doi: 10.1002/mabi.200500062.
(48) Kang Y, Chen P, Shi X, Zhang G, Wang C. Preparation of open-porous stereocomplex PLA/PBAT scaffolds and correlation between their morphology, mechanical behavior, and cell compatibility. RSC Adv. 2018;8(23):12933–43. doi: 10.1039/c8ra01305e.
(49) Ko S, Hong M, Park B, Gupta R, Choi H, Bhattacharya S. Morphological and rheological characterization of multi-walled carbon nanotube/PLA/PBAT blend nanocomposites. Polym Bull. 2009;63(1):125–34. doi: 10.3390/nano11040857.
(50) Azam MU, Samad MA. UHMWPE hybrid nanocomposite coating reinforced with nanoclay and carbon nanotubes for tribological applications under water with/without abrasives. Tribol Int. 2018;124:145–55. doi: 10.1016/j.triboint.2018.04.003.
(51) Xiang S, Feng L, Bian X, Li G, Chen X. Evaluation of PLA content in PLA/PBAT blends using TGA. Polym Test. 2020;81:106211. doi: 10.1016/j.polymertesting.2019.106211.
(52) Chow WS, Lim YT. Antistatic and thermal properties of poly (lactic acid)/polypropylene/carbon nanotube nanocomposites. J Eng Sci. 2020;16(2):57–69. doi: 10.21315/jes2020.16.2.3.
(53) Bao R-Y, Yang W, Jiang W-R, Liu Z-Y, Xie B-H, Yang M-B, et al. Stereocomplex formation of high-molecular-weight polylactide: A low temperature approach. Polym J. 2012;53(24):5449–54. doi: 10.1016/j.polymer.2012.09.043.
(54) Azizi S, Azizi M, Sabetzadeh M. The role of multiwalled carbon nanotubes in the mechanical, thermal, rheological, and electrical properties of PP/PLA/MWCNTs nanocomposites. J Compos Sci. 2019;3(3):64. doi: 10.3390/jcs3030064.